Melting and Premelting Properties for a Series of Potassium Polysulfides

George J. Janz* and Derek J. Rogers

Cogswell Laboratory, Rensselaer Polytechnic Institute, Troy, New York 12181

The melting and premelting thermal behavior has been investigated for a series of polysulfide compositions from ~45 to ~82 wt % sulfur by using the techniques of differential scanning calorimetry (DSC). The thermicity for the formation of the polysulfides from K_2S and K_2S_3 has been characterized by an in situ calorimetric technique. Enthalpy of fusion and heat capacity data are reported for the following compositions: di-, tri-, tetra-, penta-, and hexasulfides. Pronounced glass-forming tendencies on cooling from the molten state are observed in the region of ~62-~67 wt % sulfur; this composition range is also characterized by inverse crystallization phenomena, much as observed in the closely related Na_2S-sulfur system. The calorimetric studies were extended to two compositions of still higher sulfur content, i.e., ~74 and ~82 wt % sulfur, and behavioral aspects are examined in the light of the preceding results.

High-temperature thermodynamic data have recently been reported for the Na_2S-sulfur system as part of investigations of energy-related candidate salt systems for the molten sulfur electrode (*1*, *2*). In the present communication we report the results of an extension of these studies to the K_2S-sulfur system.

The status of the phase-rule studies (*3*, *4*) is summarized in Figure 1. Inspection shows the existence of five maxima and three eutectics. For the di-, tri-, penta-, and hexasulfides the maxima are well-defined; for the tetrasulfide, the maximum appears to be slightly hidden (i.e., incongruently melting composition). At compositions of 71.8 wt % sulfur and greater, there is a separation into two layers (*5*), one consisting of a saturated solution of sulfur in the hexasulfide and the other a saturated solution of the polysulfides in sulfur. Pearson and Robinson (*4*) propose that the di- and trisulfides do not melt congruently, but rather incongruently like the tetrasulfide. In the present work, investigations of the compositions of well-defined stoichiometry (i.e., the di-, tri-, tetra-, penta-, and hexasulfides), with some limited extension to compositions of sulfur content > 72 wt %, were undertaken with DSC calorimetry as the principal technique.

Investigation of the thermal properties appears limited to the work of Bousquet et al. (drop calorimetry; differential thermal analysis) (*6*). Markedly different values for the enthalpy of fusion were reported for two of these polysulfides, viz, K_2S_4 and K_2S_5, the technique of DTA leading to values ~70-250% larger than from drop calorimetry. Our principle effort thus was aimed at obtaining reliable values for the thermal properties. Our measurements were extended to the characterization of the melting-crystallization behavior for a series of increasing sulfur compositions (up to ~82 wt % sulfur) in the K_2S-sulfur system, and these results are also reported.

Experimental Section

Our high-temperature differential scanning calorimetry facility has been described in detail elsewhere (*1*). The facility centers around a Perkin-Elmer DSC-Model 2 calorimeter, together with an LMS system of microprocessor components and software (*7*) for computer-assisted data acquisition, base-line corrections, and data analysis in enthalpy and heat capacity measurements. A quantitative and accurate small mass measurement capability completes the assembly. The latter, together with the sample capsules and seal press, was housed in a dry N_2 atmosphere glovebag so that the final sample transfer and encapsulation could be completed in an inert environment.

Cross-check measurements for energy calibration were made with three metals, indium, tin, and lead, and two salt systems, KNO_3 and LiCl-KCl eutectic (*8-10*). The accuracy limits of the measurements thus established were as follows: temperatures, ±0.5 °C; heats of fusion, ±2%; heat capacities, ±2%.

For the enthalpy and heat capacity measurements, the compositions were prepared by the "in-capsule" DSC technique of this laboratory (*1*, *11*, *12*). In this method, the reactant materials are weighed in milligram amounts and in the exact stoichiometries required for the desired composition; after this the DSC sample pans are hermetically sealed. Possible contamination through trace impurities is thus minimized, if not completely bypassed. All transfers are performed in a rigorously dry inert atmosphere.

The tetra-, penta-, and hexasulfide compositions were prepared by the in-capsule DSC technique using K_2S_3 and highly refined sulfur (see ref *1*) in the required (weighed) amounts. The K_2S_3 was prepared from metallic potassium (Purified Grade; Baker Chemical Co., Inc.) and the same grade of sulfur (above) after the ethanolic technique of Pearson and Robinson (*4*). The analytical procedures of Feher and Berthold (*13*) were used to establish the exact composition (±2%) of the K_2S_3 thus gained. For K_2S_2, the in-capsule technique was also used, but with K_2S (99.9% purity; Cerac/Pure Chemicals Co., Inc.) and K_2S_3 as reactant materials. The use of K_2S and sulfur as starting materials for the preparation of the above polysulfides via the in-capsule technique was explored. This approach was found not successful. The DSC scans and enthalpy of fusion measurements confirmed that K_2S_6 is always initially formed in the preparative approach, i.e., quite irrespective of the ratios of the reactants. Subsequent solution of K_2S in molten K_2S_6 with disproportionation to lower polysulfides appears slow. Thus, the route is not recommended for the preparation of polysulfides other than K_2S_6.

The thermicity of each of the above preparative syntheses for K_2S_2, K_2S_4, K_2S_5, and K_2S_6 was investigated; the DSC scans are illustrated in Figure 2a. Completion of the reaction was taken as disappearance of the K_2S_3 or the sulfur endotherms (via repetitive scans). The DSC scans for the melting process for the polysulfides thus prepared are in Figure 2b, together with the results for elemental sulfur, and K_2S_3.

Melting temperatures were determined from the leading edge of the melting endotherms (*2*, *11*).

The enthalpies of solid-solid transitions and melting, and the heat capacities of the polysulfides as crystalline solids and in the molten (liquid) states, are summarized in Tables I-III. For these measurements, the heating and cooling rates were set at 10 °C min^{-1} with a N_2 sweep of ~20 cm^3 min^{-1} throughout the assembly. The heat capacity data were acquired in overlapping 50 °C temperature increments over the total temperature range spanned.

0021-9568/83/1728-0331$01.50/0

Table I. Enthalpy of Fusion and Solid-Solid Transitions

composition: sulfur, wt %	composition: polysulfide formula	t, °C	ΔH,[a] cal mol^{-1}
		transition: solid ⇄ solid	
45.1	K_2S_2	146	36.0
		transition: solid ⇄ melt	
45.1	K_2S_2	487	4370
55.2	K_2S_3	302	5960
62.1	K_2S_4	154	2780
67.2	K_2S_5	205	6450
71.1	K_2S_6	189	6600
74.3	$K_2S_{7.06}$	*b*	
81.6	$K_2S_{10.84}$	*b*	

[a] For conversion to SI units: 1 cal = 4.184 J. [b] Sulfur-saturated layer melts, ~118 °C; hexasulfide layer melts, ~188 °C, see Figure 4.

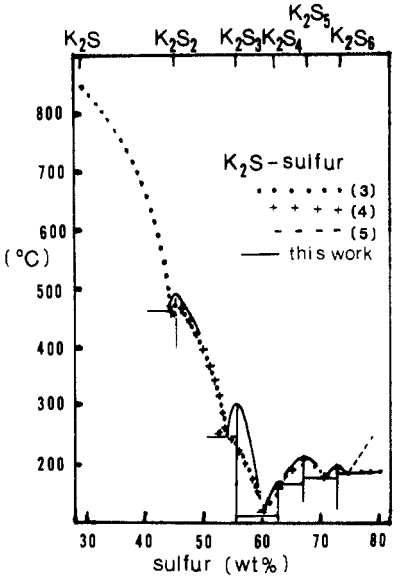

Figure 1. Phase diagram for the system K_2S–sulfur.

Table II. Heat Capacity Data[a]

t, °C	C_p, cal mol^{-1} deg^{-1}	t, °C	C_p, cal mol^{-1} deg^{-1}
	K_2S_2		
60	27.33	450	33.35
100	27.95	487	mp
200	29.49	507	38.30
300	31.03	550	38.30
400	32.58	590	38.30
	K_2S_3		
60	33.21	330	45.75
100	31.92	350	44.55
200	35.00	400	45.55
250	39.92	450	51.12
302	mp	490	58.89
	K_2S_4		
60	41.21	154	mp
100	45.28	175	55.74
120	47.31	300	55.74
130	48.33	475	55.74
	K_2S_5		
60	46.10	205	mp
100	48.71	225	69.37
150	52.00	325	69.37
170	53.31	375	69.37
	K_2S_6		
60	50.36	189	mp
100	54.45	215	73.68
150	59.56	250	73.68
160	60.59	320	73.68
	$K_2S_{7.06}$		
118	S melting	280	39.79
189	K_2S_6 melting	300	40.44
260	40.50	310	41.13
	$K_2S_{10.84}$		
118	S melting	250	20.78
189	K_2S_6 melting	270	20.62
200	21.85	280	20.60
220	21.31		

[a] For conversion to SI units, see Table I.

Results and Discussion

The temperatures, enthalpies of solid-state and melting transitions, and the heat capacities for the series of polysulfide compositions investigated are in Tables I–III. In a related communication from this labortory concerning structural studies (*14*), the macroscopic preparative synthesis and the characterization of this series by melting point data, elemental analyses, and X-ray powder diffraction data are reported (except for the three compositions K_2S_2, $K_2S_{7.06}$, and $K_2S_{10.84}$. The melting

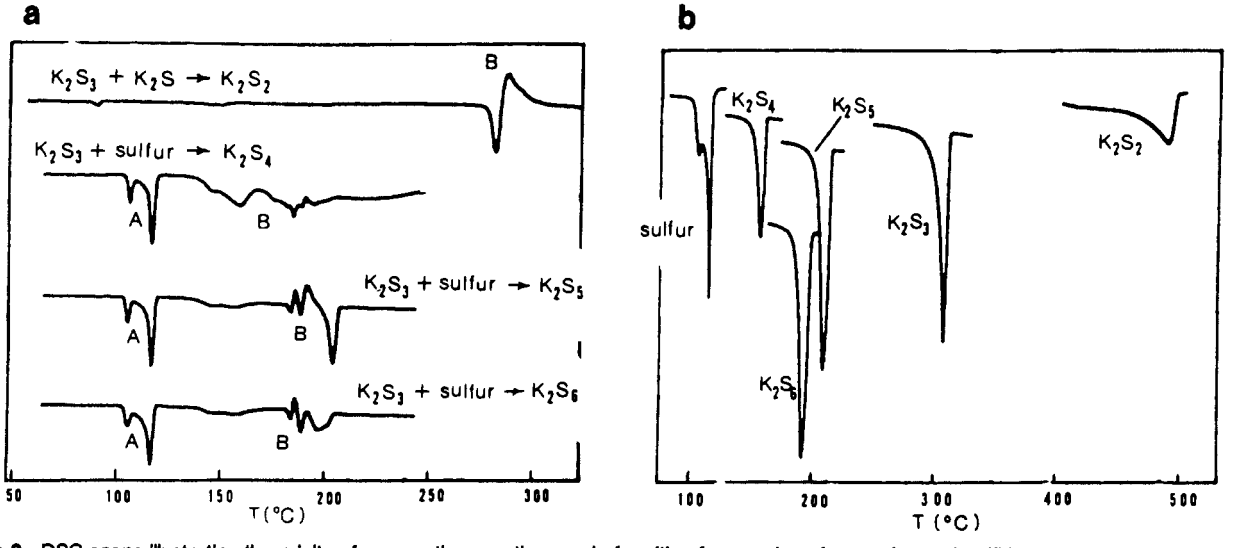

Figure 2. DSC scans illustrating thermicity of preparative reactions and of melting for a series of potassium polysulfides. (a) Thermicity of reactions observed by the in situ DSC preparative technique: (A) sulfur melting zone; (B) chemical reaction zone. (b) Fusion endotherms for sulfur and five polysulfides.

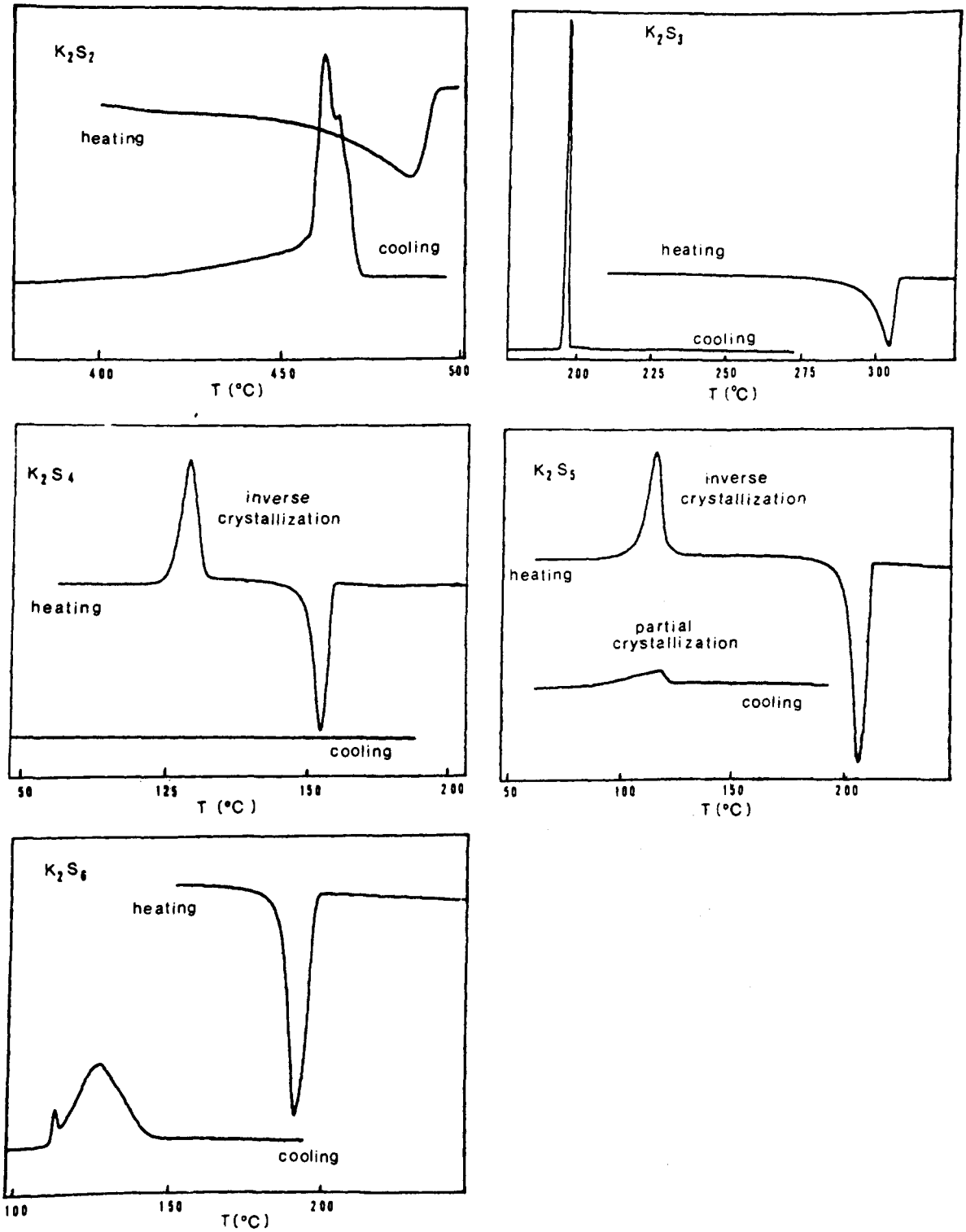

Figure 3. Melting–crystallization behavior in thermal cycling a series of potassium polysulfides. The heating and cooling DSC scans are shown for a series of polysulfides, over the temperature range from ~50 °C, through fusion, and into the molten state. The tendency to formation of the glassy state was very pronounced for K_2S_4, and somewhat less for K_2S_5; for these two compositions the crystallization exotherm onsets as these compositions are being reheated, i.e., the inverse of the crystallization behavior of well-behaved polycrystalline systems (cf. NaCl, LiCl–KCl, KNO_3, ...).

point data for the tri-, tetra-, penta-, and hexasulfides are in close accord with the earlier observations (~±3 °C); for the disulfide the limits are somewhat larger (~±5 °C). The shifts of the liquidus–solidus curve due to these results are shown in Figure 1. Examination of the diagram shows quite clearly the existence of four well-defined maxima (di-, tri-, penta-, and hexasulfides) and one (slightly) hidden maximum (tetrasulfide).

The melting–crystallization behavior is illustrated in Figure 3 for the six stoichiometric compositions and in Figure 4 for the two additional compositions of higher sulfur content. Between the tetra- and pentasulfide compositions a region had been reported in which the tendency of the molten composition to form highly supercooled amorphous masses was very marked (*3*, *4*). Cleaver et al. (*15*) report a glass transition temperature, T_g, at 42 °C for the tetrasulfide. By comparison the molten di-, tri-, and hexasulfide compositions exhibited sharp crystallization exotherms, with only little supercooling effects; i.e., these exhibited all the features of well-defined polycrystalline materials.

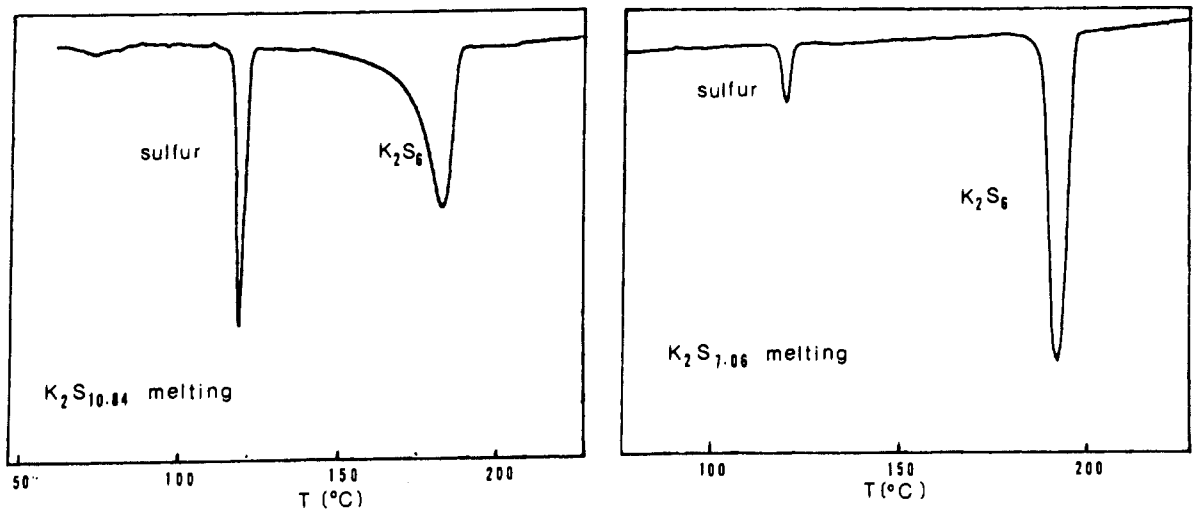

Figure 4. Thermal behavior observed for polysulfide compositions greater than 71 wt % sulfur. The DSC scans for "melting" are shown for two polysulfide compositions, $K_2S_{7.06}$ (or 74.3% sulfur) and $K_2S_{10.84}$ (or 81.6% sulfur), respectively. The behavioral pattern appears to be a composite of those of elemental sulfur and the hexasulfide; this would correspond to the formation of a region of two immiscible liquids, much as in the Na_2S–sulfur system.

Table III. Heat Capacity–Temperature Equations[a]

		$C_p = a + bt + ct^2$, cal mol^{-1} deg^{-1}		
compn	t range, °C	a	10^3b	10^6c
K_2S_2	57-450	26.404	15.436	
K_2S_3	57-252	37.873	−104.75	451.79
	327-492	169.59	−683.39	933.60
K_2S_4	57-130	35.111	101.68	
K_2S_5	57-177	42.164	65.565	
K_2S_6	57-150	44.225	102.25	
$K_2S_{7.06}$	257-310	174.257	−958.98	1709.8
$K_2S_{10.84}$	197-280	35.846	−108.80	194.14

[a] For conversion to SI units, see Table I.

This is in contrast to the Na_2S–sulfur system, in which the tendency to form highly supercooled amorphous masses (glasses) was found to be most pronounced at the trisulfide composition (*1*, *2*). The partial crystallization exhibited by some compositions (e.g., K_2S_5, Figure 3), the pronounced supercooling effects, and the onset of the crystallization exotherms on reheating the materials (i.e., "inverse" crystallization, K_2S_4; K_2S_5; Figure 3) indicate clearly the difficulties that would be encountered in obtaining trustworthy transition-point data (melting points, enthalpies, heat capacities) with techniques such as drop calorimetry and/or DTA (differential thermal analyses). As noted elsewhere, in the DSC technique, energy measurements are possible in both the melting and crystallization cycles. In the calorimetric work of Bousquet et al. (*6*), enthalpies of fusion were reported from drop calorimetry, and from DTA (differential thermal analyses). These results, together with the present work, are as follows:

	ΔH_{fus}, kcal mol^{-1}				
	K_2S_2	K_2S_3	K_2S_4	K_2S_5	K_2S_6
drop (*6*)	2.665	3.860	1.985	1.720	6.200
DTA (*6*)		3.50	3.40	6.00	6.30
DSC (present work)	4.37	5.96	2.78	6.45	6.60

Inspection shows that the results are in close accord from all three techniques for K_2S_6, and in moderately good agreement (for DTA and DSC) for K_2S_5. For K_2S_5, the difference between the drop and the differential calorimetric techniques is in the direction predicted for partial crystallization effects when the melt is cooled.

The differing results from the DTA (*6*) and the present DSC measurements are not as readily understood. Some of the differences may be due, in part, to the thermal history of the materials prior to the measurements. In the present work an in-capsule preparative technique, with K_2S_3, K_2S, and sulfur as reactants, was used to gain the various polysulfides as polycrystalline materials. The thermal data are for the melting of the polysulfides thus prepared.

The behavior of two of the above polysulfide compositions (i.e., K_2S_4 and K_2S_5) after an extended period in the molten state (~315 °C, ~800 h) was reexamined by using the DSC technique. The melting–crystallization behavior and properties for the pentasulfide were virtually the same as for the first melting cycle (i.e., melting point, ΔH_{fus}, and the melting–cooling DSC scans were as in Table I and Figure 3). For K_2S_4, the pronounced tendency to supercool was retained, but inverse crystallization had become erratic (i.e., could not be induced reproducibly in each cycle). When it could be induced, the inverse crystallization exotherm now overlapped with the onset of the melting endotherm; i.e., the inverse crystallization had shifted to somewhat higher temperatures.

For compositions having sulfur content greater than the hexasulfide, these fall in the region of liquid–liquid immiscibility. The melting behavior is summarized in Table I and in Figure 4, respectively. The melting point data (Table I) indicate very sparing solubilities of the second components. Quantitative solubility estimates were not pursued. It was found that the observed magnitudes of the enthalpies of fusion and the heat capacities could be predicted quantitatively from the known stoichiometries of these samples, and the data for sulfur (*1*) and for the hexasulfide (Tables I–III), by using the simple principles of mole fractions and state-functions additivity.

Acknowledgment

We acknowledge the participation of Giai Truong in the calorimetric measurements, and specifically for the heat capacity measurements herewith.

Registry No. K_2S_2, 1336-23-8; K_2S_3, 37488-75-8; K_2S_4, 12136-49-1; K_2S_5, 12136-50-4; K_2S_6, 37188-07-1.

Literature Cited

(1) Janz, G. J.; Rogers, D. J. *Proc. 8th Int. Symp. Thermophys. Prop.* **1981**, *2*, 626.
(2) Janz, G. J.; Rogers, D. J. *J. Appl. Electrochem.* **1982**, *13*, 121.
(3) Thomas, J. S.; Rule, S. *J. Chem. Soc.* **1914**, *105*, 177.
(4) Pearson, T. G.; Robinson, P. L. *J. Chem. Soc.* **1931**, 1304.
(5) Crosbie, G. M. *J. Electrochem. Soc.* **1982**, *129*, 2707.
(6) Bousquet, J.; LeToffe, J. M.; Diot, M. *J. Chim. Phys. Phys.-Chim. Biol.* **1974**, *71*, 1180.

(7) Chudzicki, M., Laboratory MicroSystems, Inc., P.O. Box 336, Troy, NY 12180, unpublished work, 1980.
(8) "Selected Values of Chemical Thermodynamic Properties"; National Bureau of Standards, U.S. Department of Commerce: Washington, DC, 1960; Circular 500.
(9) Janz, G. J. *J. Phys. Chem. Ref. Data* **1980**, *9*, 791.
(10) Clark, R. P. *J. Chem. Eng. Data* **1973**, *20*, 18.
(11) Rogers, D. J.; Janz, G. J. *J. Chem. Eng. Data* **1982**, *27*, 424.
(12) Rogers, D. J.; Yoko, T.; Janz, G. J. *J. Chem. Eng. Data* **1982**, *27*, 366.
(13) Feher, F.; Berthold, H. J.; Fresenius *Z. Anal. Chem.* **1953**, *138*, 245.
(14) Janz, G. J.; Coutts, J. W.; Downey, J. R.; Roduner, E. *Inorg. Chem.* **1976**, *15*, 1755.
(15) Cleaver, B.; Davies, A. J.; Hames, M. D. *Electrochem. Acta* **1973**, *18*, 719.

Received for review October 28, 1982. Accepted February 22, 1983. The work was made possible, in large part, by support received from the U.S. Department of Energy, Washington, DC.

Acidic Dissociation of Amantadine Hydrochloride

Robert I. Gelb and Daniel A. Laufer*

Department of Chemistry, University of Massachusetts, Boston, Massachusetts 02125

The acidic dissociation constants of aqueous amantadine hydrochloride have been determined by acid/base colorimetry between 25 and 50 °C using thymol blue indicator. The temperature variations of the equilibrium constants yield standard enthalpies and entropies for the acid dissociation ($\Delta H°$ = 14.15 kcal mol^{-1}; $\Delta S°$ = −0.9 cal mol^{-1} K^{-1}) and for the second indicator dissociation ($\Delta H°$ = 2.55 kcal mol^{-1}; $\Delta S°$ = −33.2 cal mol^{-1} K^{-1}).

Amantadine (adamantanamine or tricyclo[3.3.1.1^{3,7}]decan-1-amine, which will be referred to as A) has been the subject of many researches including especially its biological and medicinal uses (*1*). However, this unusual compound, which features a large rigid hydrocarbon skeleton, also affords an opportunity to study aqueous solvation phenomena with a so-called "hydrophobic species". Presumably information regarding solvation properties of A could be surmised from its acid/base properties but these have not appeared in the chemical literature. Therefore, we have undertaken to measure the thermodynamic properties of A basicity as detailed below.

Methodology

The presence of a suitable acid/base indicator in a solution allows a simple means of estimating the pH value from measurements of the absorbance. Such measurements with A, AH$^+$ solutions would yield estimates of acidity constants of AH$^+$ (or, equivalently, basicity constants of A). In order to relate the solution absorbance to pH, however, it is first necessary to "calibrate" the indicator by determining the indicator absorbance in solutions of known pH. We determined that a thymol blue indicator (thymolsulfonephthalein) and glycine buffer would be appropriate for these calibration measurements. We will abbreviate the thymol blue acid–base pair as HIn$^-$, In^{2-} and the glycine pair as HGly, Gly$^-$. Thus, we made measurements with six or seven mixtures of HGly, NaOH, and thymol blue added as NaHIn at each temperature which would be employed in later experiments with A. Absorbances were determined with 1.000-cm cells at an irradiating wavelength of 596 nm, where only the blue In^{2-} species absorbs. The data were analyzed as follows.

In each calibrating solution, the relevant equilibria are

$$K_{Gly} = \frac{a_{H^+}a_{Gly^-}}{a_{HGly}} = \frac{\gamma_H\gamma_{Gly}}{\gamma_{HGly}}\frac{[H^+][Gly^-]}{[HGly]} \quad (1)$$

$$K_{In} = \frac{a_{H^+}a_{In^{2-}}}{a_{HIn^-}} = \frac{\gamma_H\gamma_{In}}{\gamma_{HIn}}\frac{[H^+][In^{2-}]}{[HIn^-]} \quad (2)$$

$$K_W = a_H a_{OH} = \gamma_H\gamma_{OH}[H^+][OH^-] \quad (3)$$

and mass and charge balances are

$$F_{Gly} = [Gly^-] + [HGly] \quad (4)$$

$$F_{In} = [In^{2-}] + [HIn^-] \quad (5)$$

$$[Na^+] + [H^+] = [Gly^-] + [HIn^-] + 2[In^{2-}] + [OH^-] \quad (6)$$

In these equations a's and γ's denote activities and activity coefficients, respectively, of species denoted by subscripts and F_{Gly} (0.010 F throughout) and F_{In} (0.06 mF throughout) denote formal (analytical) concentrations of glycine and thymol blue. The pH value in our solutions was always high enough so that protonated H_2Gly^+ and H_2In species were negligible. The absorbance at 596 nm is related to solution concentrations by

$$A_{596} = abF_{In}([In^{2-}]/F_{In}) \quad (7)$$

These equations involve a number of assumptions and primary among these is the absence of any specific interaction between glycine species and thymol blue species. We were able to verify directly that no measurable interaction occurs between neutral glycine and HIn$^-$ present as the dominant indicator species at pH 6 by noting that the indicator spectrum over the visible range from 400 to 700 nm is unaffected by the presence of glycine at this pH. Similar experiments at very high pH precluded interactions between In^{2-} and Gly$^-$ species. Remaining possible interactions are excluded by inference from the data analysis. These interactions would presumably cause deviations from the model equations 1–7, which make no provision for them. The deviations would lead to unsatisfactorily large uncertainties in calculated parameters but these uncertainties were not observed.

In our analysis of absorbance vs. composition data we regarded K_W and K_{Gly} as known parameters whose values were obtained from ref *2* and *3*, respectively. Activity coefficients were estimated from the Debye–Hückel equation and employed the temperature-dependent parameter values given by Robinson and Stokes (*4*). Ion-size parameters of 0.35, 0.4, 0.6, and 0.9 nm were used for OH$^-$, Gly$^-$, AH$^+$, and H$^+$ ions and 0.9 nm was used for both indicator forms. Species concentrations are expressed in units of mol kg^{-1}.

The quantities that we seek in these experiments are K_{In} and abF_{In}. We proceeded interatively by first estimating K_{In} which then yielded direct solution of eq 1–7 for a_H in each measurement solution. Then, combining eq 3, 5, and 7 yields

$$1/A_{596} = (\gamma_{H_{In}})(K_{In}/abF_{In})a_H + 1/abF_{In} \quad (8)$$

A plot of $1/A_{596}$ vs. a_H yields values of K_{In}/abF_{In} and $1/abF_{In}$

0021-9568/83/1728-0335$01.50/0